PROPERTIES OF EIGENFUNCTIONS IN THE QUANTUM CANTORI REGIME*

Nazar Savytskyy, Szymon Bauch, Aleksander Błędowski
Oleh Hul, and Leszek Sirko

Institute of Physics, Polish Academy of Sciences
Lotników 32/46, 02-668 Warszawa, Poland

(Received June 3, 2002)

We study experimentally and numerically properties of quarter-stadium billiard's eigenfunctions in the regime of quantum cantori. A quarter-stadium billiard was simulated experimentally by a thin quarter-stadium microwave cavity. Experimental eigenfunctions in the cantori regime $N = 7$–63 of the quarter-stadium microwave billiard with the parameter $\varepsilon = 0.1$ were reconstructed using a field perturbation technique and a circular wave expansion method. The eigenfunctions $N = 76$–499 lying in the cantori regime of the quarter-stadium billiard with $\varepsilon = 0.05$ were investigated numerically.

PACS numbers: 05.45.Mt

It is well known that classical chaos maybe confined to the certain regions of phase space. The Kolmogorov–Arnold–Moser (KAM) theorem [1] allows us to understand that KAM tori can act as impenetrable barriers to the probability flow. However, with increasing nonlinearity of the system the KAM tori break up into cantori [2,3] and become partially penetrable to the chaotic orbits. In the seminal paper by Geisel *et al.* [4] it was shown that in quantum mechanics classical cantori appear to act as dynamical barriers that can entirely inhibit the diffusive growth. Theoretical analysis of classical and quantum properties of stadium billiards has led to identification of four different localized regimes, namely, perturbative, cantori, dynamical and ergodic [5, 6, 8]. The perturbative regime, dynamical localization regime and the ergodic regime exist also in rough billiards and were subject of intensive theoretical [9–11] and experimental [12, 13] work. Casati and Prosen [6, 7] have shown that for the quarter-stadium billiards in the quantum cantori

* Presented at the Photons, Atoms and All That, PAAT 2002 Conference, Cracow Poland, May 31–June 1, 2002.

regime ($\frac{1}{16}\varepsilon^{-2} < N < \frac{1}{16}\varepsilon^{-3}$) the rescaled localization length of the eigenfunctions is constant. This theoretical finding has been recently confirmed experimentally and numerically in [14]. In this paper we focus our attention on experimental and numerical studies of properties of eigenfunctions of a quarter-stadium billiard in the regime of quantum cantori.

Experimentally, eigenfunctions (electric field) were evaluated for the thin (height $h = 8$ mm) microwave cavity with the shape presented in Fig. 1. The microwave cavity simulates the quarter-stadium billiard with the parameter $\varepsilon = a/R = 0.1$ due to the equivalence between the Schrödinger equation and the Helmholtz equation for two-dimensional systems. This equivalence remains valid for frequencies less than the cut-off frequency $\nu_{\rm c} = c/2h \simeq 18.7$ GHz, where c is the speed of light.

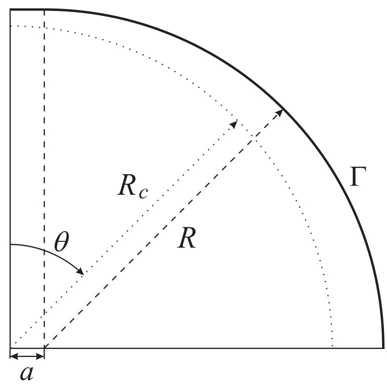

Fig. 1. The quarter-stadium billiard with radius R and straight segment a. In the experiment the quarter-stadium microwave billiard with $R = 20$ cm and $a = 2$ cm ($\varepsilon = a/R = 0.1$) was used. Squared eigenfunctions $|\Psi_N(R_{\rm c}, \theta)|^2$ were evaluated on a quarter-circle of fixed radius $R_{\rm c} = 19$ cm. Billiard's boundary Γ is marked with the bold line.

The eigenfunctions $\Psi_N(r, \theta)$ (electric field distribution $E_N(r, \theta)$ inside the cavity, N is the level number) were determined from the form of $E_N(R_{\rm c}, \theta)$ evaluated on a quarter-circle of fixed radius $R_{\rm c}$ (see Fig. 1) [14]. The perturbation technique developed in [15] and used successfully in [15–18] was implemented in measurements of $E_N(R_{\rm c}, \theta)^2$. In this method a small perturber is introduced inside the cavity to alter its resonant frequency according to

$$\nu - \nu_N = \nu_N(aB_N^2 - bE_N^2)\,, \tag{1}$$

where ν_N is the $N^{\rm th}$ resonant frequency of the unperturbed cavity, a and b are geometrical factors. Equation (1) shows that the formula can not be used to evaluate E_N^2 until the term containing magnetic field B_N vanishes. To minimize the influence of B_N on the frequency shift $\nu - \nu_N$ a dielectric perturber [19] containing a small piece of a metallic pin was used. The perturber was a dielectric sphere of 3.0 mm in diameter. A small piece of a metallic pin was introduced inside the perturber in order to move it with a magnet placed on the top of the cavity. The size of the pin (2.0 mm in length and 0.40 mm in diameter) was chosen to be the smallest possible that still allowed the perturber to follow smoothly the magnet during its movement. Relatively weak interaction between the magnet and the perturber minimized the friction between the sphere and the wall and improved accuracy of the perturber positioning inside the cavity. Additionally, for the same purpose, the inner part of the cavity's top wall was lubricated. No positive frequency shifts exceeding the uncertainty of frequency shift measurements (20 kHz) were observed with this perturber. The regime of quantum cantori for the experimental quarter-stadium billiard ($\varepsilon = 0.1$) should be observed for $N = 7$–63. Using a field perturbation technique we measured squared eigenfunctions $|\Psi_N(R_{\rm c},\theta)|^2$ for 41 modes out of 57 within the specified region. The range of corresponding eigenfrequencies was from $\nu_7 = 3.04$ GHz to $\nu_{63} = 7.59$ GHz. The measurements were performed at 2 mm steps along a quarter-circle with fixed radius $R_{\rm c} = 19$ cm. This step was small enough to reveal in details the space structure of low-lying levels. In Fig. 2 we show the examples of the squared eigenfunction $|\Psi_N(R_{\rm c},\theta)|^2$ evaluated for levels 12 and 36. The perturbation method used in our measurements allows us to extract information about the eigenfunction amplitude $|\Psi_N(R_{\rm c},\theta)|$ at any given point of the cavity but it doesn't allow to determine the sign of $\Psi_N(R_{\rm c},\theta)$ [20]. Numerical calculations performed for the quarter-stadium billiards (*e.g.*, [21]) suggest the following sign-assignment strategy: We begin with the identification of all close to zero minima of $|\Psi_N(R_{\rm c},\theta)|$. Then the sign "plus" maybe arbitrarily assigned to the region between the first and the second minimum, "minus" to the region between the second minimum and the third one, the next "plus" to the next region between consecutive minima and so on. In this way we construct our "trial eigenfunction" $\Psi_N(R_{\rm c},\theta)$. If the assignment of the signs is correct we should reconstruct the eigenfunction $\Psi_N(r,\theta)$ inside the billiard with the boundary condition $\Psi_N(r_\Gamma,\theta_\Gamma) = 0$.

As it was proposed in [6] eigenfunctions of a quarter-stadium billiard may be expanded in terms of circular waves (here only odd-odd states in expansion are considered)

$$\Psi_N(r,\theta) = \sum_{s=1}^{M} a_s C_s J_{2s}(k_N r)\sin(2s\theta)\,, \tag{2}$$

where $C_s = (\frac{\pi}{4}\int_0^{r_{\max}} |J_{2s}(k_N r)|^2 r dr)^{-1/2}$ and $k_N = 2\pi\nu_N/c$. In Eq. (2) the number of basis functions is limited to $M = k_N r_{\max}/2 = l_N^{\max}/2$, with $r_{\max} = R + a$. $l_N^{\max} = k_N r_{\max}$ is a semiclassical estimate for the maximum

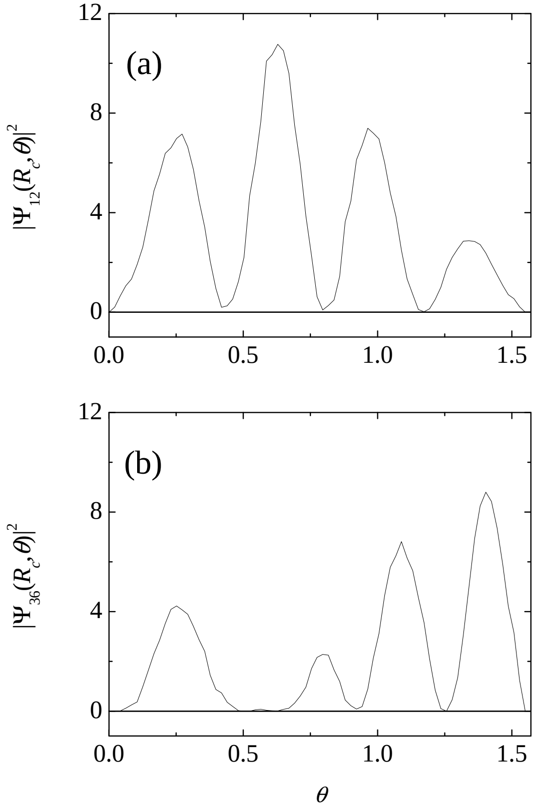

Fig. 2. Squared eigenfunctions $|\Psi_N(R_c, \theta)|^2$ (in arbitrary units) measured on a quarter-circle with radius $R_c = 19$ cm with the level numbers: (a) $N = 12$ ($\nu_{12} \simeq 3.59$ GHz), (b) $N = 36$ ($\nu_{36} \simeq 5.85$ GHz).

possible angular momentum for a given k_N. Circular waves with angular momentum $2s > 2M$ correspond to evanescent waves and can be neglected. Coefficients a_s may be extracted from the "trial eigenfunction" $\Psi_N(R_c, \theta)$ via

$$a_s = [\frac{\pi}{4} C_s J_{2s}(k_N R_c)]^{-1} \int_0^{\pi/2} \Psi_N(R_c, \theta) \sin(2s\theta) d\theta \,. \tag{3}$$

Since our "trial eigenfunction" $\Psi_N(R_c, \theta)$ is only defined on a quarter-circle of fixed radius R_c and is not normalized we imposed normalization of the coefficients a_s: $\sum_{s=1}^{M} |a_s|^2 = 1$. Now, the coefficients a_s and Eq. (2) can be used to reconstruct the eigenfunction $\Psi_N(r, \theta)$ of the billiard. Figs. 3 and 4 show reconstructed eigenfunction $\Psi_{36}(r, \theta)$ of the billiard for two different

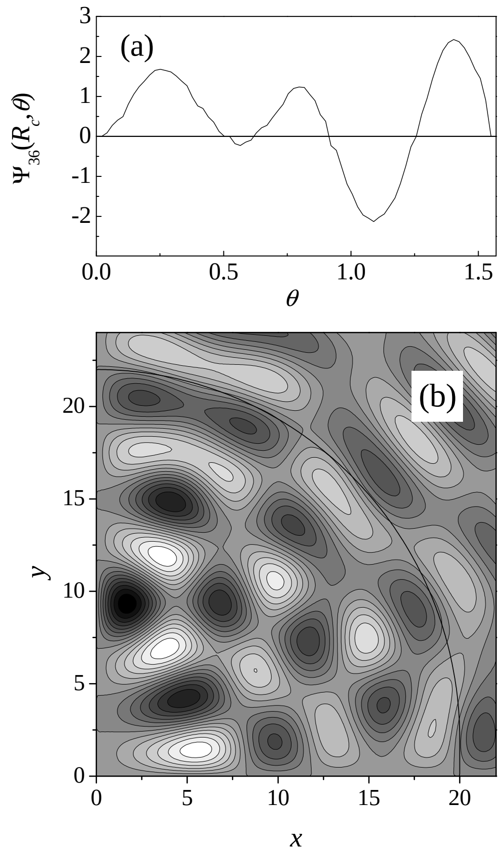

Fig. 3. Panel (a): "Trial eigenfunction" $\Psi_{36}(R_c, \theta)$ obtained from the measured $|\Psi_{36}(R_c, \theta)|^2$ using a sign assignment strategy: $(+, -, +, -, \cdots)$. Panel (b): Eigenfunction of the experimental billiard $\Psi_{36}(r, \theta)$ reconstructed from the "trial eigenfunction" $\Psi_{36}(R_c, \theta)$. The amplitudes have been converted into a grey scale with white corresponding to large positive and black corresponding to large negative values, respectively. Billiard's boundary Γ is marked with the bold line. Let us note that the eigenfunction $\Psi_{36}(r, \theta)$ has proper boundary condition: $\Psi_{36}(r_\Gamma, \theta_\Gamma) \simeq 0$ (see text).

sign assignments in the "trial eigenfunction" $\Psi_{36}(R_c, \theta)$. Due to experimental uncertainties and the finite step size in the measurements of $|\Psi_N(R_c, \theta)|^2$ the eigenfunctions $\Psi_N(r, \theta)$ are not exactly zero at the boundary Γ. As the quantitative measure of the sign assignment quality we chose the integral $\gamma \int_\Gamma |\Psi_N(r, \theta)|^2 dl$ calculated along the billiard's boundary Γ, where $\gamma = \pi R/2 + a$ is length of Γ. For the two cases in Fig. 3 and Fig. 4 we got the values of 0.04 and 0.94, respectively, that clearly show that the reconstruction of the eigenfunction $\Psi_{36}(r, \theta)$ was done properly only in the first

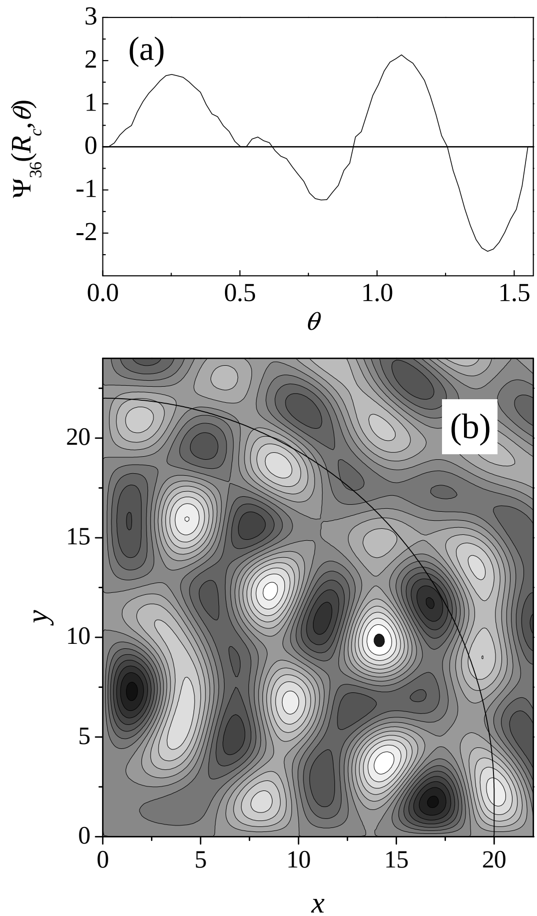

Fig. 4. Panel (a): Another "trial eigenfunction" $\Psi_{36}(R_{\rm c},\theta)$ obtained from the measured $|\Psi_{36}(R_{\rm c},\theta)|^2$. Panel (b): Eigenfunction $\Psi_{36}(r,\theta)$ reconstructed from the "trial eigenfunction" $\Psi_{36}(R_{\rm c},\theta)$ does not fulfill the boundary condition: $\Psi_{36}(r_\Gamma,\theta_\Gamma)\simeq 0$ and was rejected. The amplitudes have been converted into a grey scale with white corresponding to large positive and black corresponding to large negative values, respectively. Billiard's boundary Γ is marked with the bold line.

case (Fig. 3). Using the method of the "trial eigenfunction" we were able to reconstruct 41 experimental eigenfunctions of the quarter-stadium billiard with the level number N between 7 and 63. The remaining 16 eigefunctions from the quantum cantori region $N = 7$–63 were not reconstructed due to the problems with the measurements of $|\Psi_N(R_{\rm c},\theta)|^2$ along a quarter-circle coinciding with one of the nodal lines of $\Psi_N(r,\theta)$.

The localization length ℓ of the experimental eigenfunctions $\Psi_N(r,\theta)$ was estimated using the concept of the Shannon width [6, 22]:

$$\ell = \beta \exp(-\sum_s |a_s|^2 \ln |a_s|^2) , \tag{4}$$

where the numerical constant $\beta = 2.46$. In [14] the localization length ℓ was calculated using the definition: $\ell = 2.76 \min \{\#A; \sum_{s\in A} |a_s|^2 \geq 0.99\}$. It is so called the 99% probability localization length which is defined as the minimal number of the circular eigenfunctions that are needed to support the 99% probability of an eigenstate $\Psi_N(r,\theta)$. The numerical constant β in (4) was adjusted to give the same value of the rescaled localization length $\sigma = \ell/l_N^{\max}$ in our and [6, 7] calculations performed for the billiard with the parameter $\varepsilon = 0.05$.

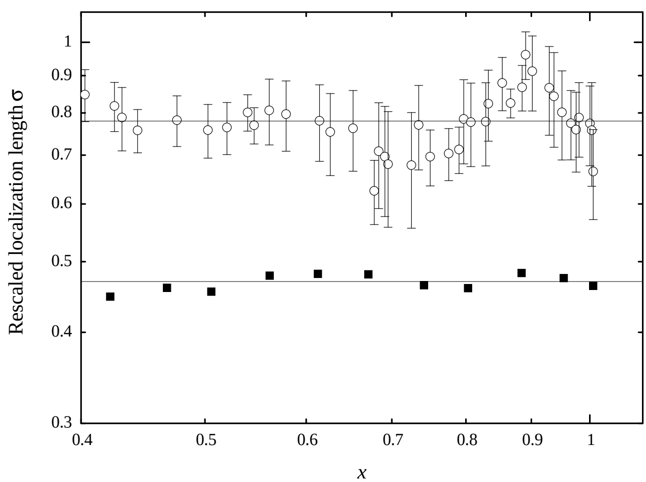

Fig. 5. Rescaled localization length $\sigma = \ell/l_N^{\max}$ versus the scaling variable $x = \varepsilon^{3/2}k_N R$ in the regime of quantum cantori. Empty circles present experimental results for the quarter-stadium billiard with $\varepsilon = 0.1$. Points were obtained by averaging over 5 eigenstates. Full line marks the average value of experimental rescaled localization length $\bar{\sigma} = 0.78 \pm 0.03$. Full squares present numerical results for the quarter-stadium billiard with $\varepsilon = 0.05$. Each point was obtained by averaging over 25 consecutive eigenstates. The full line shows the average value $\bar{\sigma} = 0.47 \pm 0.01$ obtained by averaging over 424 numerically calculated eigenstates ($N = 76 - 499$). Only selected points are shown for clarity.

In Fig. 5 we show the rescaled localization length σ calculated for the experimental eigenfunctions $\Psi_N(r,\theta)$ lying in the quantum cantori region $N = 7 - 63$ versus the scaling variable $x = \varepsilon^{3/2}k_N R$. Each point is obtained by averaging over 5 eigenstates. The least-squares fit to the experimental data gave the line whose slope 0.01 ± 0.12 agrees within the error with the expected slope of 0. The average value of the rescaled localization length was estimated to be $\bar{\sigma} \simeq 0.78 \pm 0.03$

Fig. 5 provides experimental confirmation of the predicted existence of the quantum cantori regime where the rescaled localization length of the eigenfunctions does not depend on average on the level number N. Observed fluctuating behavior of the rescaled localization length σ with the level number N was also observed in numerical calculations. It is worth to mention that in agreement with [6] the 99% probability localization length calculated in [14] gave less fluctuating results. Casati and Prosen [6] link this behavior with the property of the 99% probability which is less sensitive to the slowly decaying tails of the distributions $|a_s|^2$.

Investigation of the quantum cantori regime for billiards with smaller parameter ε requires estimation of eigenfunctions with much higher level numbers *e.g.*, $25 < N < 500$ for $\varepsilon = 0.05$. Due to experimental limitations (*e.g.*, step of 2 mm in measurements of $|\Psi_N(R_c, \theta)|^2$) we could not do it experimentally. Instead we decided to analyze such a billiard numerically. Eigenfunctions of the quarter-stadium billiard ($R = 20$ cm, $a = 1$ cm, $\varepsilon = a/R = 0.05$) were calculated using the method based on the Green function approach, BIM (the boundary integral method) [11, 23]. It was tested [11] that BIM allows for effective calculation of relatively low eigenvalues and eigenfunctions of quantum billiards ($N < 1000$) and from this point of view it can be treated as complementary to the method of Vergini and Saraceno [24] used in [6] that works very efficiently for much higher N.

We show our numerical results in Fig. 5. For the billiard with the parameter $\varepsilon = 0.05$ the rescaled localization length σ also does not depend on average on the scaling variable x. Each point in these calculations is obtained by averaging over 25 consecutive eigenstates. Such a behavior of the rescaled localization length σ strongly supports the existence of the quantum cantori regime in quarter-stadium billiards. The average value of the rescaled localization length $\bar{\sigma} \simeq 0.47 \pm 0.01$ is smaller than the one obtained for the billiard with $\varepsilon = 0.1$.

Knowledge of the billiard's eigenfunctions allows us to find the structure of the energy surface in the regime of quantum cantori. For this reason we extracted eigenfunction amplitudes $C_{nl}^{(N)} = \langle n, l | N \rangle$ in the basis n, l of a quarter-circular billiard with radius $r_{\max}$, where $n = 1, 2, 3 \ldots$ enumerates the zeros of the Bessel functions and $l = 1, 2, 3 \ldots$ is the angular quantum number. The squared amplitudes $|C_{nl}^{(N)}|^2$ and their projections into the energy surface for the representative experimental eigenfunction ($N = 36$, $\varepsilon = 0.1$) and the numerical eigenfunction ($N = 424$, $\varepsilon = 0.05$) are shown in Fig. 6(a) and Fig. 6(b), respectively. In both cases the eigenfunctions are localized in the n, l basis. The full lines on the projection planes in Fig. 6 mark the energy surface of a quarter-circular billiard $H(n,l) = E_N = k_N^2$ estimated from the semiclassical formula [13]: $\sqrt{(l_N^{\max})^2 - l^2} - l\arctan(l^{-1}\sqrt{(l_N^{\max})^2 - l^2}) + \pi/4 = \pi n$. The peaks $|C_{nl}^{(N)}|^2$ are spread almost perfectly along the line marking the energy surface. It is worth to note that in the regimes of Wigner and Shnirelman ergodicity investigated in rough billiards [11, 13] the eigenstates are extended over the whole energy surface.

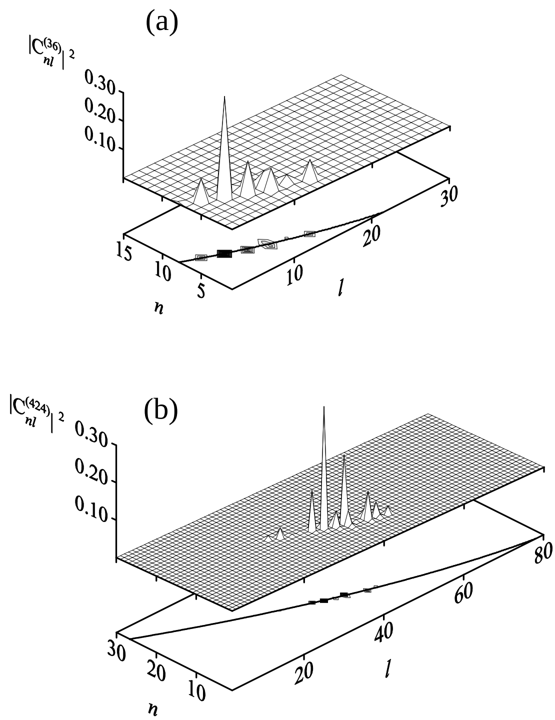

Fig. 6. Structure of the energy surface in the regime of quantum cantori. Here we show the squared amplitudes $|C_{nl}^{(N)}|^2$ for the eigenfunctions: (a) $N = 36$ ($\varepsilon = 0.1$), (b) $N = 424$ ($\varepsilon = 0.05$). In both cases the eigenfunctions are localized in the n, l basis. Full lines show the semiclassical estimation of the energy surface (see the text).

An additional confirmation of non-ergodic behavior of the measured and calculated eigenfunctions can be also sought in the form of the amplitude distribution $P(\Psi)$ [21, 25]. For irregular, chaotic states the probability of finding the value Ψ at any point inside the billiard, without knowledge of the surrounding values, should be distributed as a Gaussian, $P(\Psi) \sim \mathrm{e}^{-\beta\Psi^2}$. The amplitude distributions $P(\Psi A^{1/2})$ for the experimental eigenfunction $N = 36$ ($\varepsilon = 0.1$) and the numerical one $N = 424$ ($\varepsilon = 0.05$) are shown in

Fig. 7. They were constructed as normalized to unity histograms with the bin equal to 0.1. Each particular histogram was built using approximately 48000 values of an eigenfunction. The width of the amplitude distribution $P(\Psi)$ was rescaled to unity by multiplying normalized to unity eigenfunction by the factor $A^{1/2}$, where A denotes billiard's area (see formula (23) in [21]). For all measured and calculated eigenfunctions there is no agreement with the standard normalized Gaussian prediction $P_0(\Psi A^{1/2}) = (1/\sqrt{2\pi})\mathrm{e}^{-\Psi^2 A/2}$ (results presented in Fig. 7 are no exceptions) that strongly suggests that chaos is suppressed in the quantum cantori regime.

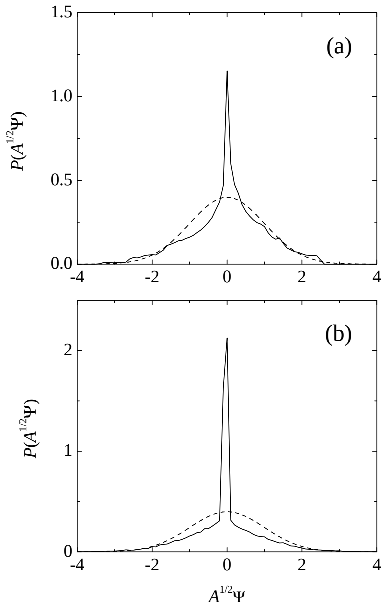

Fig. 7. Amplitude distribution $P(\Psi A^{1/2})$ for the eigenstates: (a) $N = 36$ ($\varepsilon = 0.1$) and (b) $N = 424$ ($\varepsilon = 0.05$) constructed as histograms with bin equal to 0.1. The width of the distribution $P(\Psi)$ was rescaled to unity by multiplying normalized to unity eigenfunction by the factor $A^{1/2}$, where A denotes billiard's area. Dashed line shows standard normalized Gaussian prediction $P_0(\Psi A^{1/2}) = (1/\sqrt{2\pi})\mathrm{e}^{-\Psi^2 A/2}$.

Finally we calculated the spatial correlation function [21]

$$C(\boldsymbol{x}, \boldsymbol{s}) = \frac{1}{\langle |\Psi(\boldsymbol{x})|^2 \rangle} \langle \Psi(\boldsymbol{x} + \tfrac{1}{2}\boldsymbol{s})\, \Psi^*(\boldsymbol{x} - \tfrac{1}{2}\boldsymbol{s}) \rangle \,, \tag{5}$$

where the local average $\langle \cdots \rangle$ is defined as follows:

$$\langle |\Psi(\boldsymbol{x})|^2 \rangle = \frac{1}{\Delta^n} \int\limits_{-\Delta/2}^{\Delta/2} |\Psi(\boldsymbol{x} + \boldsymbol{s})|^2 d^n s \,.$$

In the integrable circular case the spatial correlation function [21] can be calculated analytically

$$C_{l,n}(r,\theta;s,\phi) = \cos\left[l\frac{s}{r}\sin(\phi-\theta)\right]\cos\left[\frac{s}{r}\sqrt{k_{n,l}^2 r^2 - l^2}\cos(\phi-\theta)\right] , \quad (6)$$

where (r,θ) are the coordinates of a point $\boldsymbol{x}$ inside the circle billiard, s is the distance measured from $\boldsymbol{x}$, and ϕ is the angle of $\boldsymbol{s}$ relative to the positive x axis. $k_{n,l}$ is the eigenvalue of the circle billiard.

In the ergodic case the correlation function is given by

$$C_N(\boldsymbol{x},\boldsymbol{s}) = J_0(k_N s), \quad (7)$$

where k_N is the wave number of the N-th eigenfunction of the ergodic billiard.

Results of calculations of the spatial correlation function $C(\boldsymbol{x},\boldsymbol{s})$ are shown in Fig. 8 and Fig. 9.

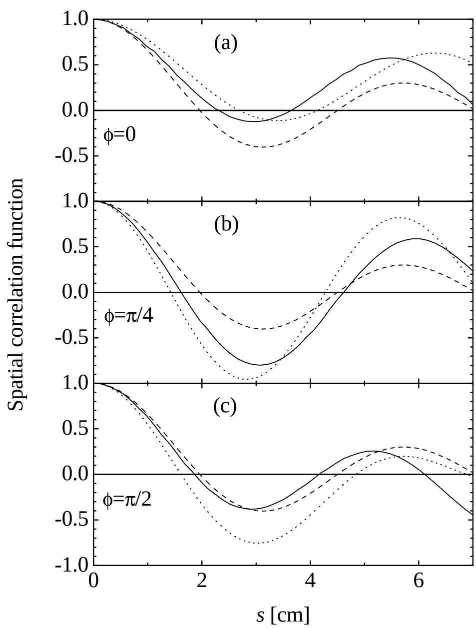

Fig. 8. The spatial correlation function $C(\boldsymbol{x},\boldsymbol{s})$ calculated for the experimental eigenfunction $N = 36$ of the stadium billiard with $\varepsilon = 0.1$. Panel (a): Full line shows the correlation function calculated for $(r,\theta) = (13.53\text{ cm}, 1.03)$ and $\phi = 0$ compared to the prediction for the ergodic billiard (dashed line) and for the integrable circle billiard (the eigenfunction with the quantum numbers $(n,l) = (6,6)$) (dotted line). Panels (b) and (c): As above but for $\phi = \pi/4$ and $\phi = \pi/2$, respectively.

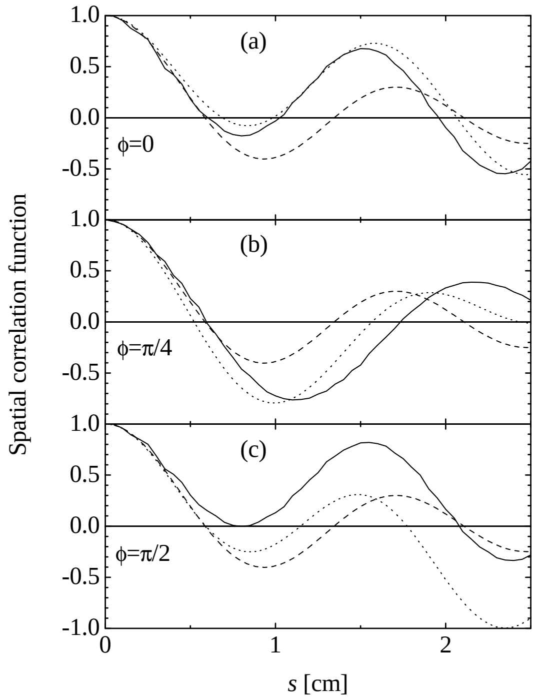

Fig. 9. The spatial correlation function $C(\boldsymbol{x}, \boldsymbol{s})$ calculated for the theoretical eigenfunction $N = 424$ of the stadium billiard with $\varepsilon = 0.05$. Panel (a): Full line shows the correlation function calculated for $(r, \theta) = (13.53\ \text{cm}, 1.03)$ and $\phi = 0$ compared to the prediction for the ergodic billiard (dashed line) and for the integrable circle billiard (the eigenfunction with the quantum numbers $(n, l) = (12, 36)$) (dotted line). Panels (b) and (c): As above but for $\phi = \pi/4$ and $\phi = \pi/2$, respectively.

The correlation function $C(\boldsymbol{x}, \boldsymbol{s})$ for the experimental eigenfunction $N = 36$ of the stadium billiard with $\varepsilon = 0.1$ is presented in Fig. 8. Figs. 8(a)–(c) show the correlation function calculated for $(r, \theta) = (13.53\ \text{cm}, 1.03)$ with $\phi = 0$, $\phi = \pi/4$ and $\phi = \pi/2$, respectively, in the function of s compared to the prediction for the ergodic billiard (7). The local average indicated in (5) were in practice carried out over an area encompassing about 1.5 wavelengths. Distribution of the squared amplitudes $|C_{nl}^{(N)}|^2$ presented in Fig. 6(a) shows that the eigenfunction $N = 36$ has mostly $(n, l) = (6, 6)$ character. Therefore, for the completeness of the comparison the correlation function $C_{l,n}(r, \theta; s, \phi)$ is also shown. The correlation function $C(\boldsymbol{x}, \boldsymbol{s})$ presented in Fig. 8 deviates from the prediction for the ergodic as well as for the integrable billiards indicating that in the cantori regime the eigenfunctions, although, being not completely ergodic are quite different from the integrable ones.

The correlation function $C(\boldsymbol{x}, \boldsymbol{s})$ for the theoretical eigenfunction $N=424$ of the stadium billiard with $\varepsilon = 0.05$ is shown in Fig. 9. The correlation function $C(\boldsymbol{x}, \boldsymbol{s})$ calculated for $(r, \theta) = (13.53\ \mathrm{cm}, 1.03)$ with $\phi = 0$, $\phi = \pi/4$ and $\phi = \pi/2$, respectively, is compared to the correlation function for the ergodic billiard (7) and to the correlation function $C_{l,n}(r, \theta; s, \phi)$ $(n, l) = (12, 36)$ for the integrable circle billiard. The quantum numbers $(n, l) = (12, 36)$ were chosen because for them the $|C_{nl}^{(N)}|^2$ distribution presented in Fig. 6(b) has its maximum. The local averages in (5) were calculated over an area encompassing about 2.5 wavelengths. Also in this case there are discrepancies between the correlation function $C(\boldsymbol{x}, \boldsymbol{s})$ calculated for the stadium billiard and the correlation functions evaluated for the ergodic and integrable systems. However, the shape of $C(\boldsymbol{x}, \boldsymbol{s})$ is more similar to the shape of the correlation function of the integrable system than the ergodic one. Such a behavior of the correlation function $C(\boldsymbol{x}, \boldsymbol{s})$ could be attributed to the smaller value of the rescaled localization length σ for the billiard with $\varepsilon = 0.05$. In the limit of the integrable circle billiard, where the formula (6) is directly applicable, $\sigma \to 1/l_N^{\max}$. We would like to remark that if the local average in $C(\boldsymbol{x}, \boldsymbol{s})$ is replaced by averaging over the whole area of a billiard $C(\boldsymbol{x}, \boldsymbol{s})$ becomes similar to the ergodic correlation function (7), independently whether a system is ergodic or integrable. It means that only the local average allows to distinguish between the systems.

In summary, we evaluated experimentally and numerically eigenfunctions for quarter-stadium billiards in the regime of quantum cantori. Using the definition of the Shannon width we confirmed that in the quantum cantori regime the rescaled localization length of the eigenfunctions fluctuates around a value that depends on the parameter ε. We demonstrated that in the regime of quantum cantori the eigenfunctions are localized in the n, l basis, the amplitude distributions $P(\Psi A^{1/2})$ are different from the standard normalized Gaussian prediction $P_0(\Psi A^{1/2}) = (1/\sqrt{2\pi})\mathrm{e}^{-\Psi^2 A/2}$ and the spatial correlation functions $C(\boldsymbol{x}, \boldsymbol{s})$ calculated for experimental and theoretical eigenfunctions deviate from the correlation functions predicted for ergodic and integrable systems.

N.S. acknowledges partial support by the Polish State Committee for Scientific Research (KBN) under grant no 2 P03B 085 22. S.B., O.H. and L.S. acknowledge partial support by the Polish State Committee for Scientific Research (KBN) under grant no 2 P03B 023 17.

REFERENCES

[1] V.I. Arnold, *Mathematical Methods of Classical Mechanics*, Springer-Verlag, New York 1989.

[2] R.S. MacKay, J.D. Meiss, I.C. Persival, *Physica D* **13**, 55 (1984).

[3] D. Bensimov, L.P. Kadanoff, *Physica D* **13**, 82 (1984).

[4] T. Geisel, G. Radons, J. Rubner, *Phys. Rev. Lett.* **57**, 2883 (1986).

[5] F. Borgonovi, G. Casati, B. Li, *Phys. Rev. Lett.* **77**, 4744 (1996).

[6] G. Casati, T. Prosen, *Physica D* **131**, 293 (1999).

[7] G. Casati, T. Prosen, *Phys. Rev.* **E59**, R2516 (1999).

[8] F. Borgonovi, P. Conti, D. Rebuzzi, B. Hu, B. Li, *Physica D* **131** 317 (1999).

[9] K. Frahm, D. Shepelyansky, *Phys. Rev. Lett.* **78**, 1440 (1997).

[10] K. Frahm, D. Shepelyansky, *Phys. Rev. Lett.* **79**, 1833 (1997).

[11] Y. Hlushchuk, A. Błędowski, N. Savytskyy, L. Sirko, *Phys. Scr.* **64**, 192 (2001).

[12] L. Sirko, Sz. Bauch, Y. Hlushchuk, P.M. Koch, R. Blümel, M. Barth, U. Kuhl, H.-J. Stöckmann, *Phys. Lett.* **A266**, 331 (2000).

[13] Y. Hlushchuk, L. Sirko, U. Kuhl, M. Barth, H.-J. Stöckmann, *Phys. Rev.* **E6304**, 6208 (2001).

[14] N. Savytskyy, L. Sirko, submitted for publication (2002).

[15] L.C. Maier, J.C. Slater, *J. Appl. Phys.* **23**, 68 (1952).

[16] S. Sridhar, *Phys. Rev. Lett.* **67**, 785 (1991).

[17] C. Dembowski, H.-D. Gräf, A. Heine, R. Hofferbert, H. Rehfeld, A. Richter, *Phys. Rev. Lett.* **84**, 867 (2000).

[18] D.H. Wu, J.S.A. Bridgewater, A. Gokirmak, S.M. Anlage, *Phys. Rev. Lett.* **81**, 2890 (1998).

[19] P.M. Koch, *Physica D* **83**, 178 (1995).

[20] J. Stein, H.-J. Stöckmann, U. Stoffregen, *Phys. Rev. Lett.* **75**, 53 (1995).

[21] S.W. McDonald, A.N. Kaufman, *Phys. Rev.* **A37**, 3067 (1988).

[22] R. Blümel, A. Buchleitner, R. Graham, L. Sirko, U. Smilansky, H. Walther, *Phys. Rev.* **A44**, 4521 (1991).

[23] I. Kosztin, K. Schulten, *Int. J. Mod. Phys.* **C8**, 293 (1997).

[24] E. Vergini, M. Saraceno, *Phys. Rev.* **E52**, 2204 (1995).

[25] M.V. Berry, *J. Phys. A* **10**, 2083 (1977).